

Transferable local pseudopotentials derived via inversion of the Kohn-Sham equations in a bulk environment

Baojing Zhou,¹ Yan Alexander Wang,² and Emily A. Carter¹

¹*Department of Chemistry and Biochemistry, Box 951569, University of California, Los Angeles, California 90095-1569, USA*

²*Department of Chemistry, University of British Columbia, 2036 Main Mall, Vancouver, BC V6T 1Z1, Canada*

(Received 7 July 2003; revised manuscript received 17 December 2003; published 23 March 2004)

The lack of accurate transferable local pseudopotentials represents one of the remaining barriers to the general application of orbital-free density functional theory (OF-DFT, a linear scaling technique). Here we report a method to generate high quality *ab initio* local pseudopotentials (LPS's) for use in condensed matter DFT calculations. We exploit the first Hohenberg-Kohn theorem, which states that the external potential is one-to-one mapped to the ground-state electron density. By employing a scheme for inverting the Kohn-Sham (KS) equations due to Wang and Parr, we iteratively solve for the KS effective potential $v_{\text{eff}}^{\text{KS}}(\mathbf{r})$ until it reproduces a target density. From $v_{\text{eff}}^{\text{KS}}(\mathbf{r})$ we derive a global LPS for the entire system. This global LPS is then further decomposed to obtain an atom-centered LPS. We show that LPS's derived from bulk environments are substantially more transferable than those derived from atoms alone. In KS-DFT tests on Si, we show that this bulk-derived LPS can reproduce accurately phase orderings predicted by nonlocal pseudopotentials for both metallic and semiconducting phases. We then tested this LPS in OF-DFT calculations on Si crystals, where we demonstrate that this bulk-derived LPS (BLPS), combined with a linear-response-based kinetic energy density functional with a density-dependent kernel, correctly predicts a diamond structure ground state for Si in an OF-DFT calculation. Other bulk properties, such as defect formation energies and transition pressures are also presented as tests of this BLPS. This approach for deriving LPS's isolates much of the remaining error in OF-DFT to the kinetic energy density functional, providing means to test new functionals as they become available.

DOI: 10.1103/PhysRevB.69.125109

PACS number(s): 71.15.Dx, 71.15.Mb, 31.15.Ar

I. INTRODUCTION

The original Hohenberg-Kohn (HK) theorems of density functional theory (DFT) do not rely on the existence of a wave function to describe the physical system.¹ The density, a function of 3 instead of $3N$ coordinates, is the only physical variable. Kohn and Sham introduced a set of orbitals in order to represent the noninteracting kinetic energy as the expectation value of the Laplacian.² As a result, in the orbital-based Kohn-Sham (KS) scheme, a set of coupled nonlinear one-particle Schrödinger-like equations must be solved and one now has again $3N$ degrees of freedom to account for. By contrast, in the orbital-free (OF) DFT, one only needs to solve a single Thomas-Fermi-Hohenberg-Kohn (TFHK) equation¹

$$\frac{\delta E[\rho]}{\delta \rho(\mathbf{r})} = \frac{\delta T[\rho]}{\delta \rho(\mathbf{r})} + \frac{\delta E_{\text{ne}}[\rho]}{\delta \rho(\mathbf{r})} + \frac{\delta E_{\text{ee}}[\rho]}{\delta \rho(\mathbf{r})} = \mu. \quad (1)$$

The traditional KS-DFT method has a cost scaling cubically with the size of the system, due to the need to orthogonalize the KS orbitals. Over the past decade, there has been a blossoming of so-called linear-scaling techniques,³⁻⁵ whose objective is to reduce this cubic scaling. The orbital-based linear-scaling methods³ all depend on the “nearsightedness” principle⁵ and the concept of “locality” in quantum chemistry,⁶ which allows orbital localization into regional domains to be achieved. However, the localized orbitals within each regional domain still must be orthogonalized, which again is a $O(N^3)$ procedure, albeit with smaller N . As a result, only for large numbers of atoms (e.g.,

> 50–100 atoms or so) will these orbital-based linear-scaling methods become cheaper than the conventional canonical methods.⁵ Furthermore, these orbital-based linear-scaling strategies are not linear for metallic systems, since the orbitals in metals cannot be exponentially localized.

An alternative is to completely avoid introducing KS orbitals and instead solve directly for the density, as in the original Thomas-Fermi-Dirac-Weizsäcker (TFDW) model.⁷⁻¹¹ Then if one employs three-dimensional periodicity, it is possible to calculate the kinetic energy, external energy, and Hartree terms in reciprocal space using fast Fourier transforms, leading to effectively linear [$O(N \ln N)$] scaling.^{4,12} [Calculation of the exchange-correlation term is already $O(N)$ because it is short-ranged in real space.] Thus, in practice one can solve for the electron densities, structures, and properties of hundreds and even thousands of atoms with an OF-DFT.^{4,13-17}

The main advantage of OF-DFT is that it completely avoids the bottlenecks present in the orbital-based linear-scaling methods, such as the cost to localize and orthogonalize the orbitals and, with only a density to solve for, there is no need for Brillouin-zone integration in periodic systems. As a result, unlike the localized orbital methods, no crossover point exists in terms of system size at which the method becomes cheaper than the conventional canonical method. From the smallest system upward, the OF-DFT approach is always effectively linear scaling.

On the other hand, as a consequence of giving up the KS orbitals, the entire energy functional must be expressed solely in terms of the density, not only for the exchange and

correlation energy, but also for the kinetic energy. Development of kinetic energy density functionals (KEDF) has seen a resurgence of interest, with significant progress made especially in the last decade.^{10–12,14,15,18,19} High quality KEDF's based on the weighted density approximation (WDA) and the average density approximation (ADA) have been applied with encouraging results to atomic species and jellium surfaces.^{10,11} However, general, effective implementations of these complicated but more universal KEDF's based on the nonlocal density approximation (NLDA), for realistic molecular and periodic systems, have not been reported yet. Linear-response-based KEDF's, which rely on the so-called simplified nonlocal density approximation (SNDA), have been shown to be accurate (to the meV/atom range) for *sp*-bonded nearly free-electron-like metals (alkalis, alkaline earths, group III metals).^{4,12,14–19} However, SNDA KEDF's do not achieve meV accuracy for systems with localized electron densities such as in molecules and covalent or ionic solids. For those systems, no simple yet accurate KEDF's are available and the representation of the kinetic energy poses difficulties. This limits the accuracy of OF-DFT and hence its widespread application. Developing accurate KEDF's for these systems remains at the frontiers of research.¹²

The other technical challenge associated with general applicability of OF-DFT is the electron-nuclear interaction energy. In KS-DFT, this is often treated by nonlocal pseudopotentials (NLPS's) that contain orbital-based projection operators.^{20–22} Although transferable accurate NLPS's are available, they cannot be used in OF-DFT, since the projectors cannot act on a density instead of a wave function. This limits the form of the ion-electron interaction to be of the LPS variety [$v(\mathbf{r})$], for which it is difficult to provide transferability, i.e., LPS's may work well in one environment but not another. In this paper, we address this second issue, i.e., how to develop transferable first-principles-based LPS's for the OF-DFT method.

II. THEORY OF *ab initio* LOCAL PSEUDOPOTENTIALS

Pseudopotentials are used ubiquitously in solid state DFT calculations in order to reduce the expense associated with representing the core electrons.²⁰ Instead of explicitly considering all electrons in the system, one can often get away with explicitly considering only the valence electrons, since they are largely responsible for most physical and chemical properties of interest. The effect of the inner shell core electrons and the nuclei on the valence electrons can instead be described by a pseudopotential. There are two kinds of pseudopotentials: nonlocal (NLPS) (Refs. 20–22) and local (LPS).^{23–25} An LPS is a simple function of electron position, while an NLPS depends not only on the electron position but also utilizes a different potential for each angular momentum channel. Mathematically, this is realized by means of projection operators that act on the system's wave function, in order to project out the potential appropriate for various types of electrons (e.g., *s*, *p*, or *d*).²¹ Generally, *ab initio* NLPS's have been designed by requiring that the pseudopotential reproduce the atomic valence eigenvalues from all-electron calculations and that the pseudoatomic wave function match

the all-electron wave function beyond a chosen core cutoff radius r_c . With an appropriately chosen core radii for each l channel, calculations using an NLPS generally can reproduce the results of all-electron calculations very well. The success of the NLPS's can be attributed to the fact that the NLPS's are constructed to reproduce the valence eigenvalues and to preserve the scattering properties of the all-electron atom. Since an LPS acts on each angular momentum channel with same potential, there is no way to have such a potential reproduce all the valence eigenvalues. Therefore, the demanding requirements made of a NLPS must be altered when constructing an LPS.

A natural alternative is to devise a scheme which requires the LPS to reproduce a given valence pseudodensity.^{12,24,25} This idea is consistent with the basic tenet of DFT: only the electron density is of fundamental importance.²⁶ In the approach we describe below, no constraints are placed on the functional form of the LPS other than that it should retain a pure Coulombic tail asymptotically, so that the usual matching conditions between pseudo-wave-functions and all-electron wave functions will hold. Thus, unlike other earlier model LPS's,²³ there are no empirically fit parameters involved at all.

The first *ab initio* LPS's based on this density-reproducing concept were devised by Watson *et al.*²⁴ In their approach, the LPS's were required to reproduce a KS density within an OF-DFT calculation on a bulk crystal. To achieve this, the KS density was inserted into the TFHK equation [Eq. (1)] in OF-DFT, and then the TFHK equation was inverted in reciprocal space to obtain the reciprocal space pseudopotential $v_{\text{ext}}(\mathbf{g})$ as

$$v_{\text{ext}}(\mathbf{g}) = \left. \frac{\delta E_{ne}[\rho]}{\delta \rho(\mathbf{g})} \right|_{\rho_{\text{KS}}} = - \left. \left[\frac{\delta T[\rho]}{\delta \rho(\mathbf{g})} + \frac{\delta E_{ee}[\rho]}{\delta \rho(\mathbf{g})} \right] \right|_{\rho_{\text{KS}}}. \quad (2)$$

The LPS's resulting from this approach have certain drawbacks. First, any defect in the KEDF potential will be retained in the resulting LPS, as seen in Eq. (2). Second, these LPS's do not have a strict Coulombic tail in real space asymptotically. Finally, current KEDF's are only accurate for main group metals; therefore this precludes generalizing this approach to produce accurate LPS's for all elements.

In order to avoid the errors associated with incorporating the KEDF potential into the pseudopotential via Eq. (2), we instead construct LPS's using the exact (noninteracting) kinetic energy T_s calculated within KS theory. We first implemented this idea for atoms, i.e., producing LPS's based on a KS valence electron density for an atom.²⁵ The resulting atomic LPS's (denoted here as ALPS) are good, but still lack transferability and sufficient accuracy when applied to crystals. The motivation of the present work is to move beyond an ALPS to achieve the desired accuracy for condensed matter calculations. To accomplish this, we choose bulk crystalline KS densities as target densities that our pseudopotentials need to reproduce, as in the approach of Watson *et al.* However, here errors in the KEDF potential do not appear, since the exact T_s potential is employed. We term the resulting potential the bulk LPS (BLPS). We will see that the BLPS yields results significantly superior to those using the ALPS.

III. *ab initio* LOCAL PSEUDOPOTENTIAL DERIVED FROM BULK CRYSTALS

According to the first HK theorem,¹ a unique LPS exists one-to-one mapped to a given ground-state density. Therefore, given a high-quality density, we simply require a path between the density and the potential. However, there is no unique path—this is an example of the “inverse problem” in mathematics. Many paths have been suggested;^{27,28} we have found that an approach suggested by Wang and Parr²⁷ is the most stable numerically and therefore we employ it here.

In order to start construction of the LPS, we must have a high quality target density that we wish to reproduce—the extent to which the LPS we create is able to achieve this will be the figure of merit by which we judge the quality of the LPS. Here, we employ the Troullier-Martins (TM) NLPS (Ref. 22) in order to generate the target density from a KS-DFT calculation of a bulk crystal. Then the global KS potential for the entire crystal is determined from the target density following Wang-Parr’s approach. After this, the Hartree and exchange-correlation potentials are subtracted to obtain a local, global external potential. Finally, we extract an atom-centered local pseudopotential from the global external potential, as explained below.

In the Wang-Parr method,²⁷ the KS equations are inverted to solve for the potential corresponding to a given density. The following is an adaptation of the Wang-Parr method for a bulk environment. We start from the KS equations

$$\left(-\frac{1}{2}\nabla^2 + v_{\text{eff}}(\mathbf{r})\right)\phi_{i,k} = \epsilon_{i,k}\phi_{i,k}, \quad (3)$$

where i is the band index and k is the index of \mathbf{k} points. Specifically, our goal is to find the LPS contained within the local KS effective potential $v_{\text{eff}}(\mathbf{r})$ in Eq. (3) that reproduces a target density. We do so by multiplying both sides of Eq. (3) by $(\phi_{i,k}^*/\epsilon_{i,k})$, then summing over all the bands and \mathbf{k} points, and then dividing by $\bar{\rho}(\mathbf{r})$, the energy-weighted density

$$\bar{\rho}(\mathbf{r}) = \sum_k w(k) \sum_i f_{i,k} \frac{|\phi_{i,k}(\mathbf{r})|^2}{\epsilon_{i,k}}. \quad (4)$$

Here, $w(k)$ is the weight associated with each \mathbf{k} point and $f_{i,k}$ is the occupation number of the orbital $\phi_{i,k}$. This leads to an exact expression for the local KS effective potential (which implicitly contains the desired LPS) given by

$$v_{\text{eff}}(\mathbf{r}) = \frac{\rho(\mathbf{r}) + \sum_k w(k) \sum_i f_{i,k} \phi_{i,k}^*(\mathbf{r}) \left(\frac{1}{2}\nabla^2\right) \phi_{i,k}(\mathbf{r}) / \epsilon_{i,k}}{\bar{\rho}(\mathbf{r})}. \quad (5)$$

While $\rho(\mathbf{r})$, the target density, is an *input* from a *separate* self-consistent field calculation (in our case, KS-DFT using a TM NLPS on the same bulk crystal), the occupation numbers $f_{i,k}$, the eigenvalues $\epsilon_{i,k}$ and the orbitals $\phi_{i,k}$ in Eq. (5) are unknown initially for the LPS case; they must be obtained for the case of KS-DFT with an LPS. Therefore Eq. (5) cannot be used directly and an iterative solution must be employed. This was designed by Wang and Parr as the following: at the n th iteration, the KS equations are solved with the last iteration’s version of the KS potential $v_{\text{eff}}^{n-1}(\mathbf{r})$ which contains the $(n-1)$ th’s LPS, to obtain orbitals and eigenvalues for the next iteration

$$\left(-\frac{1}{2}\nabla^2 + v_{\text{eff}}^{n-1}(\mathbf{r})\right)\phi_{i,k}^n(\mathbf{r}) = \epsilon_{i,k}^n \phi_{i,k}^n(\mathbf{r}). \quad (6)$$

Multiplying by $\phi_{i,k}^{n*}(\mathbf{r})$ and rearranging Eq. (6) yields

$$\phi_{i,k}^{n*}(\mathbf{r}) \left(\frac{1}{2}\nabla^2\right) \phi_{i,k}^n(\mathbf{r}) = [v_{\text{eff}}^{n-1}(\mathbf{r}) - \epsilon_{i,k}^n] |\phi_{i,k}^n(\mathbf{r})|^2. \quad (7)$$

Inserting Eq. (7) into Eq. (5) produces an approximation for the next iteration of the KS potential

$$v_{\text{eff}}^n(\mathbf{r}) = \frac{\rho(\mathbf{r}) + \sum_k w(k) \sum_i f_{i,k} [v_{\text{eff}}^{n-1}(\mathbf{r}) - \epsilon_{i,k}^n] |\phi_{i,k}^n(\mathbf{r})|^2 / \epsilon_{i,k}^n}{\bar{\rho}^n(\mathbf{r})}. \quad (8)$$

We may further simplify Eq. (8) by noticing that the first term in the summation appearing in the numerator is $v_{\text{eff}}^{n-1}(\mathbf{r}) \cdot \bar{\rho}^n(\mathbf{r})$ and the second term is the current iteration’s density $\rho^n(\mathbf{r})$. We can pull out the first term in the summation to obtain

$$\begin{aligned} v_{\text{eff}}^n(\mathbf{r}) &= v_{\text{eff}}^{n-1}(\mathbf{r}) + \frac{\rho(\mathbf{r}) - \rho^n(\mathbf{r})}{\bar{\rho}^n(\mathbf{r})} \\ &= v_{\text{eff}}^{n-1}(\mathbf{r}) + \Delta v^n(\mathbf{r}). \end{aligned} \quad (9)$$

Special attention must be paid to this quantity $\Delta v^n(\mathbf{r})$, which is the difference between the current iteration’s potential and the next iteration’s potential. First, the potential is improved in the right direction only when the energy-weighted density $\bar{\rho}^n(\mathbf{r})$ is negative everywhere; otherwise the next iteration’s potential will be worse. In order to see this, suppose the potential $v_{\text{eff}}^{n-1}(\mathbf{r})$ of $(n-1)$ th step produces a density $\rho^n(\mathbf{r})$ at \mathbf{r} , which is smaller than $\rho(\mathbf{r})$, the target density at the same point. From Eq. (9), it is obvious that if the energy-weighted density $\bar{\rho}^n(\mathbf{r})$ is positive at \mathbf{r} then $\Delta v^n(\mathbf{r})$ will also be positive, which means the next itera-

tion's potential $v_{\text{eff}}^n(\mathbf{r})$ will be more repulsive. This will lead to an even smaller density $\rho^{n+1}(\mathbf{r})$ at the next step, which is worse than the previous step.

We also observe that as $\rho^n(\mathbf{r})$ approaches closer and closer to the target density $\rho(\mathbf{r})$, $\Delta v^n(\mathbf{r})$ will get smaller and smaller. To achieve fast convergence, the energy-weighted density $\bar{\rho}^n(\mathbf{r})$ should be controlled to be small enough that $\Delta v^n(\mathbf{r})$ still has significant magnitude so that the Wang-Parr scheme remains numerically sensitive.

In order to guarantee that the energy-weighted density $\bar{\rho}^n(\mathbf{r})$ is both negative and small everywhere, we shift all eigenvalues $\epsilon_{i,k}$ by $-\epsilon_0$. This is equivalent to calculating $\bar{\rho}^n(\mathbf{r})$ from the following, instead of from Eq. (4):

$$\bar{\rho}^n(\mathbf{r}) = \sum_k w(k) \sum_i f_{i,k}^n \frac{|\phi_{i,k}^n(\mathbf{r})|^2}{\epsilon_{i,k}^n + \epsilon_0^n}. \quad (10)$$

If we use Eq. (10) in Eq. (9), this is basically the same approximation as using Eq. (4). The subtle difference is that now the approximation is weighted by $1/(\epsilon_{i,k} + \epsilon_0)$ instead of $1/\epsilon_{i,k}$. We do not need to worry about any artifact caused by the shift, as long as the final global effective potential $v_{\text{eff}}^{\text{KS}}(\mathbf{r})$ can reproduce our target density, since we know from the first HK theorem that the local potential will be determined only to within an additive constant.

The value of $-\epsilon_0$ can be chosen in an optimal manner as follows. Notice that in the summation of Eq. (10), different terms make differently sized contributions to $\bar{\rho}^n(\mathbf{r})$. The term with the smallest denominator will dominate. Based on this observation, we designed a scheme to determine the optimal value of the shift $-\epsilon_0$ at each iteration step. We first check the spacing between the eigenvalues $\epsilon_{i,k}$ of all the occupied orbitals and find the pair of adjacent energy levels with the largest gap. By carefully choosing an appropriate $-\epsilon_0$ in this gap, we can guarantee that the energy-weighted density $\bar{\rho}^n(\mathbf{r})$ is negative and small everywhere due to cancellation between oppositely-signed contributions from the selected pair of levels. We found that Wang-Parr's method works very well in a bulk environment after we control the energy-weighted density in this way, where we update the global bulk external potential $v_{\text{loc}}^{\text{global}}(\mathbf{r})$ in real space for a primitive cell. We note that for isolated atoms, $\bar{\rho}^n(\mathbf{r})$ is always negative since the eigenvalues are always negative. Moreover, convergence in the atomic case was found to be more robust than in the bulk case, so for both reasons no shift of the eigenvalues was needed for construction of an ALPS.²⁵

After the global KS effective potential is converged, the terms due to electron-electron interactions are removed to obtain the unscreened ionic pseudopotential

$$v_{\text{loc}}^{\text{global}}(\mathbf{r}) = v_{\text{eff}}^{\text{global}}(\mathbf{r}) - \frac{\delta J[\rho]}{\delta \rho(\mathbf{r})} - \frac{\delta E_{\text{xc}}[\rho]}{\delta \rho(\mathbf{r})}. \quad (11)$$

Here $J[\rho]$ and $E_{\text{xc}}[\rho]$ are the usual Hartree repulsion and exchange-correlation energies. Equation (11) provides a glo-

bal bulk ionic pseudopotential $v_{\text{loc}}^{\text{global}}(\mathbf{r})$, which is a superposition of the contributions from all the ions in the simulation cell.

We extract the atom-centered local pseudopotential $v_{\text{loc}}^{\text{atom}}(\mathbf{r})$ from $v_{\text{loc}}^{\text{global}}(\mathbf{r})$ as follows. $v_{\text{loc}}^{\text{global}}(\mathbf{r})$ is Fourier-transformed into reciprocal space

$$v_{\text{loc}}^{\text{global}}(\mathbf{g}) = \frac{1}{\Omega} \int_{\Omega} v_{\text{loc}}^{\text{global}}(\mathbf{r}) \cdot e^{i\mathbf{g} \cdot \mathbf{r}} d\mathbf{r}, \quad (12)$$

where Ω is the periodic unit cell volume. Due to the periodicity of the system, the reciprocal space external potential $v_{\text{loc}}^{\text{global}}(\mathbf{g})$ obtained by fast Fourier transform²⁹ at each iteration step should always vanish where the structure factor $S(\mathbf{g})$ (Ref. 30) is zero. Numerically, we found that sometimes this is not true, though the deviation is small. To avoid these spurious values, we set $v_{\text{loc}}^{\text{global}}(\mathbf{g})$ to zero, wherever $S(\mathbf{g})$ is zero. Next we divide $v_{\text{loc}}^{\text{global}}(\mathbf{g})$ by the structure factor $S(\mathbf{g})$ to get the form factor $v^{\text{atom}}(\mathbf{g})$,³⁰ which contains all the information of the atom-centered potential

$$v^{\text{atom}}(\mathbf{g}) = \frac{v_{\text{loc}}^{\text{global}}(\mathbf{g})}{S(\mathbf{g})}. \quad (13)$$

For an ordered bulk crystal, the Bragg vectors \mathbf{g} are discontinuous.³¹ Consequently, information is only available at the Bragg vectors of that specific bulk structure. In order to gain as much data as possible to define the BLPS, we perform the Wang-Parr iterative scheme for multiple bulk structures so as to define $v^{\text{atom}}(\mathbf{g})$ at as many \mathbf{g} vectors as possible. We then spherically average $v^{\text{atom}}(\mathbf{g})$ to get a one-dimensional isotropic pseudopotential $v_{\text{bulk}}(g)$

$$v_{\text{bulk}}(g) = \frac{1}{n_g} \sum_{|\mathbf{g}_i|=g} v^{\text{atom}}(\mathbf{g}_i), \quad (14)$$

where n_g is the total number of \mathbf{g} vectors which have the same length g . In order to most sensitively process the $v(g)$ data (especially for small g , since the Coulombic contribution becomes dominant there), we temporarily remove the Coulombic part of $v_{\text{bulk}}(g)$ to get a modified form factor $v'_{\text{bulk}}(g)$:

$$v'_{\text{bulk}}(g) = v_{\text{bulk}}(g) + \frac{4\pi Z}{g^2}, \quad (15)$$

where Z is the screened ionic charge (nuclear charge plus core electron charge).

To build in the maximum transferability into the BLPS, we require it to match the $v'_{\text{bulk}}(g)$ data from multiple bulk structures or be as close to them as possible. To achieve this, we use a smoothed cubic spline to interpolate between the $v'_{\text{bulk}}(g)$ data in order to obtain a smooth curve that best fits the raw data.

Special emphasis should be placed on the value of $v'(g=0)$, which is not uniquely defined. Although the value there will not affect either the orbitals or the density, it does affect the total energy. Its contribution to the total energy is given by

$$N_{\text{el}}\Omega^{-1}\sum_{\alpha}N_{\alpha}v'_{\alpha}(g=0), \quad (16)$$

where N_{el} is the total number of electrons in the system, N_{α} is the number of ions of species α , $v'_{\alpha}(g=0)$ is the non-Coulombic part of the pseudopotential due to the ion of species α , and Ω is the volume of the simulation cell. Thus, the value of $v'(g=0)$ is of extreme importance for our BLPS. After guessing a value for $v'(g=0)$, we interpolate and obtain a smooth cubic spline. Restoration of the Coulombic part of $v'(g)$ produces a rough reciprocal space BLPS $v_{\text{rough}}(g)$, which then can be used to carry out KS calculations.

We find that the results are very sensitive to the value of $v_{\text{rough}}(g)$ at small g , especially at the first several Bragg vectors \mathbf{g} of different bulk structures. Since the pseudopotential is completely undefined at g values less than the smallest Bragg vector, we are free to choose those values of $v'(g)$ for g 's below the first Bragg vector however we like. We therefore tune the arbitrary value of $v'(g)$ at $g=0$ and at some small g values [leaving the raw $v'_{\text{bulk}}(g)$ data untouched], until the BLPS reproduces to the best extent possible the bulk properties of several phases calculated with the NLPS.

We contrast our approach with the earlier work of Watson *et al.*,²⁴ where instead of using multiple bulk structures, a single bulk structure is employed. For the arbitrary values of $v'(g)$ at small g , they assumed an analytic Gaussian form Ae^{-bg^2} for the reciprocal space pseudopotential at low g including $g=0$. The parameters A and b were obtained by matching the value of $v^{\text{atom}}(g)$ at the lowest Bragg vector and matching the total energies from OF-DFT and KS-DFT calculations. We did not adopt this approach for several reasons. First, the shape of the reciprocal space pseudopotential at low g is not necessarily Gaussian. Second, there is no special reason to require the total energy from OF-DFT with a LPS to be the same as that from KS-DFT using a NLPS. Finally, even if we could determine the value of $v^{\text{atom}}(g=0)$ following the same approach, it is not guaranteed to be the optimal value (as defined in the Wang-Parr sense).

Since it is not enforced, this BLPS $v_{\text{rough}}(g)$ does not have a strict Coulombic tail asymptotically when transformed into real space, even though it should contain one. Unfortunately, it is almost impossible to exactly transform the one-dimensional BLPS $v_{\text{rough}}(g)$ from reciprocal space to real space directly because it is a long-range function without an analytical form. There is also numerical error or random noise in the $v_{\text{rough}}(g)$ data. Before we explain how to circumvent this problem, we emphasize our requirements for the final BLPS. First, the real space BLPS $v_{\text{BLPS}}(r)$ should have an exact Coulombic tail. Second, the numerical Fourier transform of $v_{\text{BLPS}}(r)$ should be almost the same as the $v_{\text{rough}}(g)$ we obtained before, especially for small g . In order to achieve these, the ALPS is needed in the real space construction. The following is the strategy we employ to obtain the final BLPS:

(i) We calculate $\Delta v(g)$, which is the difference between the rough BLPS and the Wang-Parr-derived ALPS (Ref. 25) in reciprocal space as

$$\Delta v(g) = v_{\text{rough}}(g) - v_{\text{ALPS}}(g). \quad (17)$$

We found that $\Delta v(g)$ dies off when g becomes large, so we take $\Delta v(g)=0$ for large g .

(ii) We numerically Bessel-Fourier transform the short range $\Delta v(g)$ to real space to get $\Delta v(r)$

$$\Delta v(r) = \frac{1}{2\pi^2} \int_0^{\infty} \Delta v(g) g \frac{\sin(gr)}{r} dg. \quad (18)$$

We found that $\Delta v(r)$ also dies off when r becomes large, which is reasonable since both the ALPS $v_{\text{ALPS}}(r)$ and the final BLPS $v_{\text{BLPS}}(r)$ should have a strict Coulombic tail in real space asymptotically. However, the numerical inaccuracy in $v_{\text{rough}}(g)$ causes some random noise in $\Delta v(r)$. We carefully choose an optimal radial cutoff r_c [by balancing transferability, which tends to reduce r_c , against the value of $v_{\text{BLPS}}(g=0)$, which tends to increase r_c] and assume that $\Delta v(r)$ vanishes beyond r_c .

(iii) We add the short range $\Delta v(r)$ to the real space ALPS $v_{\text{ALPS}}(r)$.

Now a real-space pseudopotential is obtained and it has a strict Coulombic tail (our first requirement mentioned above). We denote this intermediate level BLPS as $v_{\text{inter}}(r)$. We transform it to reciprocal space to form $v_{\text{inter}}(g)$. However, this is still not the final BLPS we desire, because some discrepancies still exist between its reciprocal space form $v_{\text{inter}}(g)$ and $v_{\text{rough}}(g)$ which violates our second requirement stated above. However, compared to the ALPS, $v_{\text{inter}}(r)$ is closer to the desired final BLPS $v_{\text{BLPS}}(r)$. We repeat the above procedure by replacing the ALPS with the intermediate level LPS $v_{\text{inter}}(g)$ in Eq. (17) and iterate further. At the end, we obtain another real space LPS, which not only has a Coulombic tail but also is nearly identical to $v_{\text{rough}}(g)$ when transformed to reciprocal space. We take this as our final BLPS. We denote its real space form as $v_{\text{BLPS}}(r)$ and its reciprocal space form as $v_{\text{BLPS}}(g)$, given by

$$v_{\text{BLPS}}(g) = 4\pi \int_0^{\infty} v_{\text{BLPS}}(r) r \frac{\sin(gr)}{g} dr. \quad (19)$$

The above procedure works because the difference between the BLPS and the ALPS is small, essentially a perturbation. However, in the next section, we will see that this small change to the original Wang-Parr-derived ALPS leads to a significant improvement in accuracy.

IV. CALCULATIONAL DETAILS

Our first application of the above scheme to generate transferable local pseudopotentials focuses on silicon. It is a particularly challenging case for a LPS, due to directional covalent bonding present in its ground-state structure. If we can successfully derive a transferable LPS for Si with this approach, it suggests other elements with directional bonding may be treatable with similar success.

In all our calculations (KS- and OF-DFT), we use the local density approximation (LDA) for electron exchange and correlation, based on the quantum Monte Carlo results of

TABLE I. KS-DFT-LDA optimized structures of hexagonal diamond (HD), complex bcc (cbcc), β -tin, body-centered tetragonal (bct5), and hcp Si.

	Space group	Lattice vectors	Fractional coordinates
HD	$P6_3/mmc-D_{6h}^4$	$\frac{c}{a} = 1.656$ $\alpha = \beta = 90^\circ, \gamma = 120^\circ$	$\pm(\frac{1}{3}, \frac{2}{3}, z); \pm(\frac{2}{3}, \frac{1}{3}, \frac{1}{2} + z)$ $z = 0.0631$
cbcc	$Ia3-T_h^7$	$\frac{c}{a} = 1.0$ $\alpha = \beta = \gamma = 90^\circ$	$(0, 0, 0; \frac{1}{2}, \frac{1}{2}, \frac{1}{2})$ $\pm(x, x, x)(\frac{1}{2} + x, \frac{1}{2} - x, \bar{x})$ $(\bar{x}, \frac{1}{2} + x, \frac{1}{2} - x)(\frac{1}{2} - x, \bar{x}, \frac{1}{2} + x)$ $x = 0.1003 \pm 0.0008$
β -tin	$I4_1/amd-D_{4h}^{19}$	$\frac{c}{a} = 0.5516$ $\alpha = \beta = \gamma = 90^\circ$	$(0, 0, 0; \frac{1}{2}, \frac{1}{2}, \frac{1}{2}) \pm (0, \frac{1}{4}, \frac{3}{8})$
bct5	$I4/mmm-D_{4h}^{17}$	$\frac{c}{a} = 1.8276$ $\alpha = \beta = \gamma = 90^\circ$	$(0, 0, 0; \frac{1}{2}, \frac{1}{2}, \frac{1}{2})$ $+ (0, 0, z), (0, 0, \bar{z})$ $z = 0.19169$
hcp	$P6_3/mmc-D_{6h}^4$	$\frac{c}{a} = 1.6$ $\alpha = \beta = 90^\circ, \gamma = 120^\circ$	$(0, 0, 0), (\frac{2}{3}, \frac{1}{3}, \frac{1}{2})$

Ceperley and Alder,³² as parametrized by Perdew and Zunger.³³

A. Bulk structures

Many different bulk structures of Si have been proposed and examined previously. Here we study the following structures: cubic diamond (CD), hexagonal diamond (HD), complex bcc (cbcc), β -tin, body-centered tetragonal (bct5),³⁴ simple cubic (sc), simple bcc (sbcc), face-centered cubic (fcc), and hexagonal-close-packed (hcp).^{35,36} The first four structures are observed experimentally,³⁶ with CD Si the most stable. We find two are semiconductors (CD and HD), and the rest are metals, consistent with other experimental or theoretical studies.³⁴⁻³⁶ Here we apply the Wang-Parr inversion method to the structures mentioned above, except for the cbcc and bct5 structures, which will be used to provide subsequent tests of the LPS.

Since the value of c/a and the fractional coordinates of HD, cbcc, β -tin, and hcp Si are not completely fixed by their symmetry, we obtained them by structural optimization in CASTEP (Ref. 37) using the LDA and the TM NLPS (discussed below). The resulting structures are used to construct and test our BLPS (Table I). The LDA-NLPS structures deviate only slightly from experiment.³⁶ As for the other four phases of bulk Si, the ratio between different lattice vectors and the fractional coordinates are fixed and need not be optimized. To reduce the computational cost in KS-DFT calculations, primitive cells are used, containing 2, 4, 8, 2, 4, 1, 1, 1, 2 atoms for CD, HD, cbcc, β -tin, bct5, sc, sbcc, fcc, and hcp Si, respectively. In OF-DFT calculations, orthorhombic unit cells of 8, 8, 16, 4, 4, 8, 2, 4, 4 atoms are used for the above structures, respectively.

B. Building the pseudopotential

In our work, three PS's are involved: the TM NLPS, the ALPS, and the BLPS. The TM NLPS was generated using

the FHI98PP DFT atomic code.³⁸ The TM NLPS was built for the $3s^2 3p^2$ ground state of Si atom. The core cutoff radii used for s -, p -, and d - angular momentum channels were 1.704, 1.878, and 2.02 Bohr, respectively. The same code was modified to build the ALPS, by forcing the ALPS to reproduce the atomic valence density obtained from the TM NLPS,²⁵ according to the Wang-Parr iterative scheme.

The BLPS was built using the CASTEP (Ref. 37) code, which was modified to apply the Wang-Parr method to bulk crystals. The Monkhorst-Pack scheme³⁹ was employed to generate special \mathbf{k} points for Brillouin-zone sampling. Fermi surface smearing (width of 0.1 eV) and a large number of \mathbf{k} points are required for metallic phases, in order to properly describe the Fermi surface. In order to obtain converged energies and densities in KS-DFT, we needed to use the following number of \mathbf{k} points in the irreducible Brillouin-zone (IBZ): 72, 56, 68, 84, and 48 for primitive unit cells of β -tin, sc, sbcc, fcc, and hcp structures, respectively. For the semiconducting phases, CD and HD Si, less \mathbf{k} points are needed in the IBZ: 28 for the former and 24 for the latter, in primitive unit cells. A high kinetic energy cutoff for the plane wave basis of 960 eV is used to ensure convergence of the density, especially for the semiconducting phases of Si. We chose the ALPS from our previous work²⁵ as the initial guess for the bulk local pseudopotential.

C. Testing the pseudopotential in bulk environments with KS-DFT

We then tested the ALPS and the resulting BLPS within KS-LDA for various bulk phases of Si, including some phases and defect structures outside the set used to build the BLPS. The CASTEP (Ref. 37) code was used again for these KS-LDA calculations. The number of \mathbf{k} points used in the IBZ here are 28, 36, 60, 120, 112, 84, 120, 84, and 64 for primitive cells of the CD, HD, cbcc, β -tin, bct5, sc, sbcc, fcc,

TABLE II. Deviations of the KS-BLPS density from the target KS-NLPS density for CD and fcc Si at the beginning and end of the Wang-Parr iterations, as checked by the four energy differences (meV/atom) described in the text.

	ΔJ		$J[\Delta\rho]$		ΔE_{xc}		$\Delta\langle v_{xc} \rho\rangle$	
	initial	final	initial	final	initial	final	initial	final
CD	-200.00	-3.56	5.45	0.14	41.60	2.17	54.50	2.75
fcc	-1.30	-0.55	0.14	0.0025	-4.01	-0.17	-5.29	-0.24

and hcp structures, respectively. Here, more \mathbf{k} points are needed to converge the total energy of these phases (when building the BLPS, we only need to ensure that the density is well converged). Using a kinetic energy cutoff of 760 eV, we found that the total energy is converged to within 0.004 eV/atom and 0.014 eV/atom for semiconducting and metallic phases of Si, respectively.

For the calculations of vacancy and interstitial defects, we employed a cubic supercell containing 64 atoms, constructed by putting together eight cubic unit cells of CD Si. The vacancy was created by removing an atom at the center of the supercell, while the self-interstitial defect was generated by putting an extra atom at the tetrahedral site.⁴⁰ The cell and ionic coordinates of both systems were not allowed to relax. A kinetic energy cutoff of 760 eV was employed. A $2\times 2\times 2$ mesh was used for the BZ sampling, as in other first-principles studies.⁴⁰

D. Application of the pseudopotential in bulk environments with OF-DFT

As mentioned earlier, the main reason to develop these LPS's is for use in linear-scaling OF-DFT calculations. Therefore, our final "acid test" is to use the ALPS and the BLPS in OF-DFT, in order to see if these LPS's, combined with linear-response-based SNDA KEDF's, can yield reasonable results for various phases of Si.

These SNDA KEDF's have the following structure:

$$T_s^{\text{SNDA}}[\rho] = T_{\text{vW}}[\rho] + T_x^{\text{SNDA}}[\rho]. \quad (20)$$

The second term can be decomposed further into two terms as

$$T_x^{\text{SNDA}}[\rho] = T_{\text{TF}}[\rho] + \sum_{\alpha,\beta} \lambda_{\alpha,\beta} C_{\text{TF}} \times \langle \rho^\alpha(\mathbf{r}) | w_{\alpha,\beta}(\mathbf{r}-\mathbf{r}') | \rho^\beta(\mathbf{r}') \rangle. \quad (21)$$

Here, the kernel $w_{\alpha,\beta}(\mathbf{r}-\mathbf{r}')$ in the nonlocal term of Eq. (21) can be either density independent (DI) or density dependent (DD). For both cases, α and β are adjustable exponents and different options are available. If the kernel is DI, then we have the Wang-Teter (WT) KEDF (Ref. 18) when $\alpha=\beta=\frac{5}{6}$, the Perrot KEDF (Ref. 14) when $\alpha=\beta=1$, the Smargiassi-Madden (SM) KEDF (Ref. 15) when $\alpha=\beta=\frac{1}{2}$, and the Wang-Govind-Carter (WGC) KEDF (Ref. 19) with a DI kernel for other choices of α and β . In the last case, up to three terms were included in the summation, where $\lambda_{\alpha,\beta}$ is the corresponding weight associated with each term and

where $\sum \lambda_{\alpha,\beta} = 1$. Up to now, the only SNDA KEDF that has a DD kernel was designed by Wang *et al.* in 1999.¹⁹ The kernel has the following structure:

$$w_{\alpha,\beta}^\gamma(\mathbf{r},\mathbf{r}',\mathbf{r}-\mathbf{r}') = w_{\alpha,\beta}[\zeta_\gamma(\mathbf{r},\mathbf{r}'),\mathbf{r}-\mathbf{r}'], \quad (22)$$

$$\zeta_\gamma(\mathbf{r},\mathbf{r}') = \left(\frac{k_F^\gamma(\mathbf{r}) + k_F^\gamma(\mathbf{r}')}{2} \right)^{1/\gamma}, \quad (23)$$

$$k_F(\mathbf{r}) = [3\pi^2\rho(\mathbf{r})]^{1/3}, \quad (24)$$

where $k_F(\mathbf{r})$ and $\zeta_\gamma(\mathbf{r},\mathbf{r}')$ are local one-body and nonlocal two-body Fermi wave vectors. In the following, we will call this WGC KEDF with a DD kernel simply the WGC KEDF. We use the WGC KEDF, with optimized¹⁹ parameters $\{\alpha,\beta\}_\gamma = \{\frac{5}{6} \pm \sqrt{5}/6\}_{2,7}$. In our OF-DFT calculations, a kinetic energy cutoff of 1520 eV is employed to converge the density for all phases. As is typical, wave vectors up to twice as large as that used to represent the wave function are required for convergence. In our OF-DFT calculations, a second order damped dynamics method^{12,19} is employed to minimize the total energy. We set the convergence criterion to be 0.125 meV/atom for all OF-DFT calculations except for HD Si, in which an even less strict convergence criterion of 0.5 meV/atom was used. If a more strict convergence criterion is used, the total energy of the semiconducting phases of Si sometimes diverges. This has been traced to numerical instabilities that sometimes arise in the WGC KEDF, as will be reported in detail elsewhere.⁴¹ For comparison, we also present results using the WT KEDF.¹⁸

V. RESULTS AND DISCUSSION

A. Building the pseudopotential

When we apply the Wang-Parr method, four criteria are used to check the convergence of the global KS effective potential $v_{\text{eff}}^{\text{global}}(\mathbf{r})$ [Eq. (9)].

(i) The difference between Hartree energies of the target density $\rho(\mathbf{r})$ and the current iteration's density $\rho^n(\mathbf{r})$, $\Delta J = J[\rho^n(\mathbf{r})] - J[\rho(\mathbf{r})]$.

(ii) The Hartree energy of the density difference $J[\Delta\rho(\mathbf{r})]$, where $\Delta\rho(\mathbf{r}) = \rho^n(\mathbf{r}) - \rho(\mathbf{r})$.

(iii) The difference between exchange-correlation energies $\Delta E_{xc} = E_{xc}[\rho^n(\mathbf{r})] - E_{xc}[\rho(\mathbf{r})]$.

(iv) The difference between exchange-correlation potential energies $\Delta\langle v_{xc}|\rho(\mathbf{r}) \rangle = \langle \rho^n(\mathbf{r}) | v_{xc}[\rho^n(\mathbf{r})] \rangle - \langle \rho(\mathbf{r}) | v_{xc}[\rho(\mathbf{r})] \rangle$, where $v_{xc}[\rho(\mathbf{r})] = \delta E_{xc}[\rho(\mathbf{r})] / \delta\rho(\mathbf{r})$.

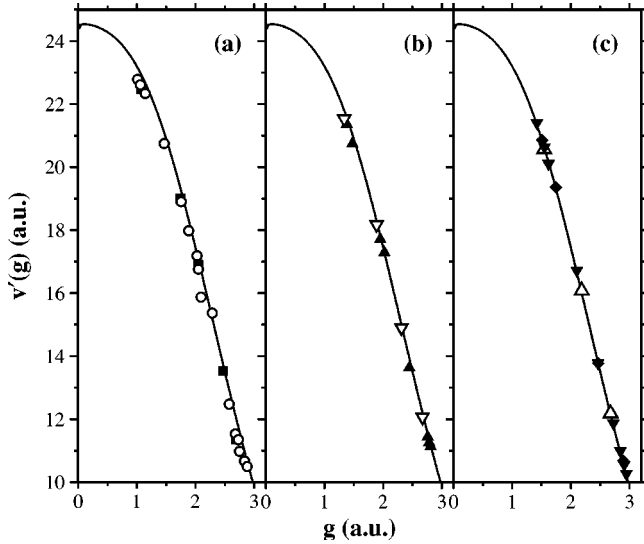


FIG. 1. Comparison of the non-Coulombic part of the ALPS (solid line) to $v'_{\text{bulk}}(g)$ data (symbols) for (a) cubic and hexagonal diamond Si (solid squares and open circles), (b) β -tin and sc Si (solid triangles and open triangles), and (c) sbcc, fcc, and hcp Si (open triangles, solid diamonds, and solid triangles).

As an example, the value of these quantities at the beginning and the end of the iterations for CD and fcc Si are shown in Table II. In both cases, all four quantities decrease by one or two orders of magnitude. Note that unlike in (spherically symmetric) atomic cases, the target density cannot be exactly reproduced by our spherically symmetric BLPS, since the bulk crystal density is, of course, not spherically symmetric.

The Wang-Parr method applied to seven bulk phases of Si yields our $v_{\text{bulk}}(g)$ and $v'_{\text{bulk}}(g)$ data (see Sec. III). The corresponding non-Coulombic part of the ALPS and the $v'_{\text{bulk}}(g)$ data from these seven bulk phases of Si are shown in Fig. 1. The ALPS matches $v'_{\text{bulk}}(g)$ of the sbcc, fcc, and hcp phases very well [Fig. 1(c)]. However, the ALPS overestimates $v'_{\text{bulk}}(g)$ of the β -tin and sc phases [Fig. 1(b)], and severely overestimates $v'_{\text{bulk}}(g)$ of the CD and HD phases at several Bragg vectors [Fig. 1(a)]. The comparison here discloses the defects in the ALPS and convinces us that constructing a BLPS that further improves upon the ALPS is worth pursuing.

By following the procedures of Sec. III, we constructed the BLPS, both in real space and in reciprocal space. The reciprocal space and real space ALPS and BLPS are plotted in Figs. 2 and 3, respectively. For comparison, we also plot the real space TM NLPS in Fig. 3. The ALPS, BLPS, and TM NLPS (all three channels) are enforced to be Coulombic-like beyond 3.5, 4.86, and 3.457 Bohr, respectively. The BLPS radial cutoff r_c of 4.86 Bohr was chosen by varying r_c to be as small as possible to enhance transferability, but it could not be chosen too small or the value of $v_{\text{BLPS}}(g=0)$ would deteriorate. The local pseudopotentials match the s channel of the nonlocal pseudopotential beyond 1.2 Bohr. For shorter distances, the LPS's strike a compromise between the s and p channels of the NLPS, though ultimately at distances within 0.5 Bohr, the LPS's become much more

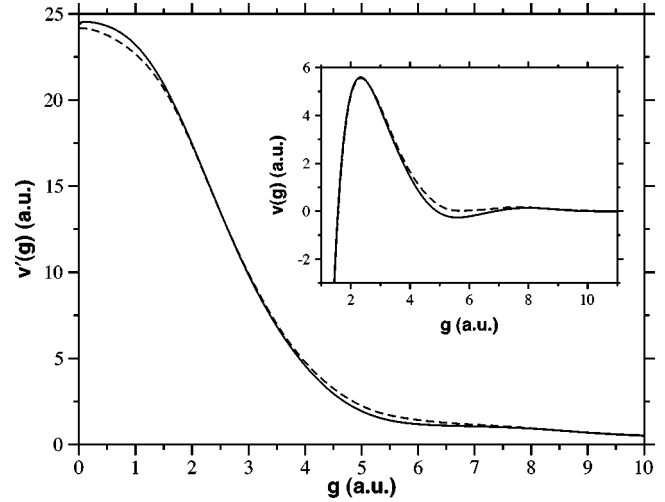


FIG. 2. Non-Coulombic part of the reciprocal space local pseudopotential for Si: the ALPS (solid line) and the BLPS (dashed line). The full reciprocal space pseudopotential containing the Coulombic part is plotted in the inset: the ALPS (solid line) and the BLPS (dashed line). Significant deviations are evident at intermediate g vectors.

repulsive. We believe this is due to the need to force the higher angular momentum electrons out from the core region. This is accomplished mathematically in an NLPS by having electrons of different angular momentum experience different potentials. The LPS's compensate for this lack of flexibility by becoming more repulsive near the nucleus.

B. Testing the pseudopotential in bulk environments with KS-DFT

We now apply our BLPS within KS-DFT to bulk crystals, comparing the results to those employing a standard TM NLPS, as well as the Wang-Parr-derived ALPS.²⁵

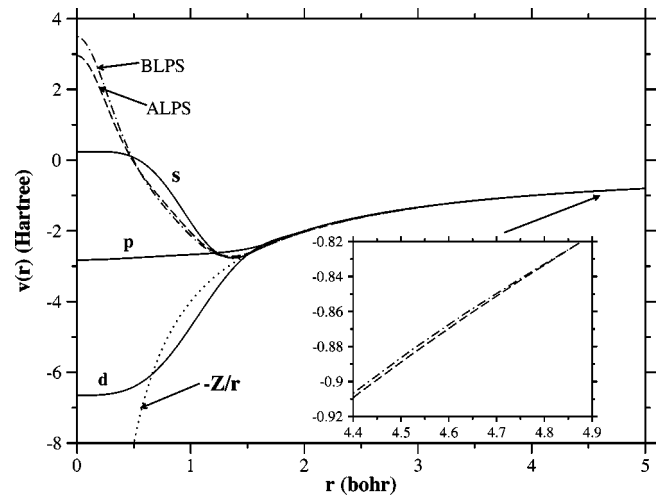


FIG. 3. Comparison of real space pseudopotentials for Si: TM NLPS (solid lines), the ALPS (dashed line), and the BLPS (dashed-dotted line). The Coulombic tails appear beyond 3.457, 3.5, and 4.86 Bohr for the TM NLPS, ALPS, and BLPS, respectively.

TABLE III. Deviations of the LPS KS-LDA densities from the NLPS KS-LDA density for CD, bct5, and fcc Si, as characterized by the four energy differences (meV/atom) described in the text.

	ΔJ	$J[\Delta\rho]$	ΔE_{xc}	$\Delta\langle v_{xc} \rho\rangle$
ALPS				
CD	-202.45	5.45	41.58	54.70
bct5	-113.89	2.79	28.33	37.25
fcc	-5.45	0.21	-1.24	-1.63
BLPS				
CD	20.34	2.04	-23.98	31.41
bct5	34.35	0.84	-20.66	-27.12
fcc	14.11	1.01	-16.64	-21.89

1. The density

By construction, the BLPS produces a more accurate density than the ALPS for various phases of Si in KS-LDA calculations. We first examine the density-related quantities outlined above, namely, ΔJ , $J[\Delta\rho]$, ΔE_{xc} , and $\Delta\langle v_{xc}|\rho\rangle$ as measures of how close the densities from the LPS's compare to that from the NLPS. Better reproduction of the NLPS KS density by the LPS KS densities will result in smaller values of those quantities. Results are shown for CD, bct5, and fcc Si in Table III. In KS-LDA, the quality of the density for CD and fcc phases obtained from the BLPS is more balanced than that from the ALPS; nevertheless, the density of fcc Si is better described than that of CD Si, which is not surprising, given that the more isotropic nature of the density in fcc Si is easier to reproduce with a LPS. Unlike the CD and fcc phases, the bct5 structure was not used to construct the BLPS, but its density using the BLPS is still significantly closer to that from the NLPS than the ALPS. This convinces us that the BLPS generally produces better densities than the ALPS for all bulk structures within KS-LDA.

We also directly compared the densities in the (110) plane of CD Si obtained using KS-LDA with the NLPS, the ALPS, and the BLPS. Figure 4(a) displays the density using the NLPS; the directional bonding between the Si atom and its nearest neighbors is evident in the highly localized regions (dark areas) of high density. The maximum valence density

in between two Si atoms reaches 0.08685 a.u. Figure 4(b) shows KS densities along the diagonal direction of the (110) plane. Within KS-LDA, the BLPS density (maximum: 0.08616 a.u.) is a bit closer to the NLPS density than is the ALPS density (maximum: 0.08570 a.u.); both reproduce the NLPS density very well.

2. Static structural properties

The quality of the LPS's also can be judged by calculating the potential energy surface (PES) for various phases. The total energy versus volume curves for bulk phases of Si using the NLPS, the ALPS, and the BLPS are plotted in Fig. 5. The insets show scaled results, where we scale the volumes by the appropriate $1/V_0$ and shift the total energies by the appropriate $-E_{\min}$, in order to directly compare the shapes of the PES's. In KS-LDA, the PESs from the ALPS and the BLPS are almost parallel to those from the TM NLPS. The corresponding insets show that the PES's from the BLPS are slightly closer to those from the NLPS in both cases.

Then the results are least-squares-fitted to Murnaghan's equation of state⁴²

$$E_{\text{tot}}(V) = \frac{B_0 V}{B'_0} \left(\frac{(V_0/V)^{B'_0}}{B'_0 - 1} + 1 \right) + \text{const.} \quad (25)$$

Here, B_0 and B'_0 are the bulk modulus and its pressure derivative at the equilibrium volume V_0 . Table IV displays the values for V_0 , B_0 , E_{\min} , and ΔE_{\min} derived from the fits, where E_{\min} is the equilibrium total energy for the CD structure and ΔE_{\min} is the energy difference $E_{\min}(\text{phase}) - E_{\min}(\text{CD})$ between the other eight structures of Si and ground state CD Si.

Use of the ALPS in KS-LDA calculations yields accurate equilibrium volumes and a phase ordering that is correct, except for the β -tin phase. However, the ALPS severely underestimates (by about a factor of 2) the energy difference between the semiconducting and most metallic phases. This is not surprising, since the values of the ALPS are too high at all Bragg vectors of the semiconducting phases of Si, while the corresponding ALPS values for the metallic phases are very good (see Fig. 1). The semiconducting phases are disfavored as a result. We can understand this by recalling that

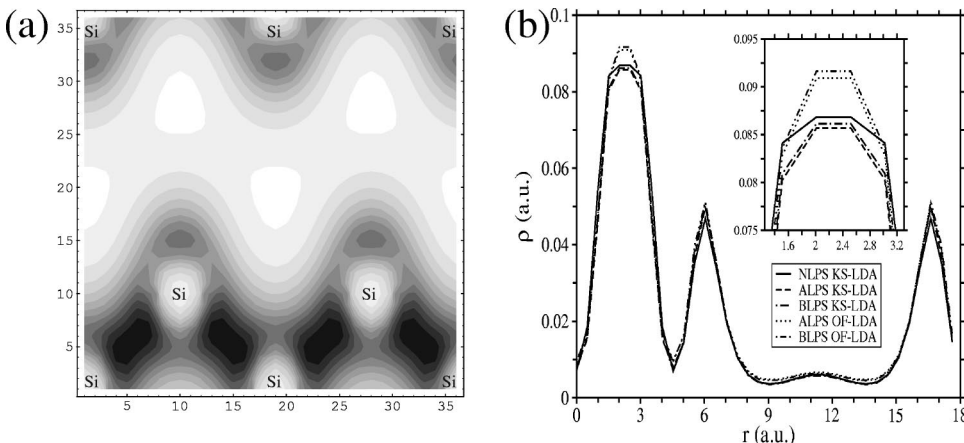


FIG. 4. LDA densities in the (110) plane of cubic diamond Si. (a) Contour plot of the density from a NLPS KS calculation. Dark areas represent high density, light areas low density. (b) Density slices along the diagonal of the (110) plane. The solid line is NLPS KS; dashed line is ALPS KS; dashed-dotted line is BLPS KS; dotted line is ALPS OF; dashed-double-dotted line is BLPS OF.

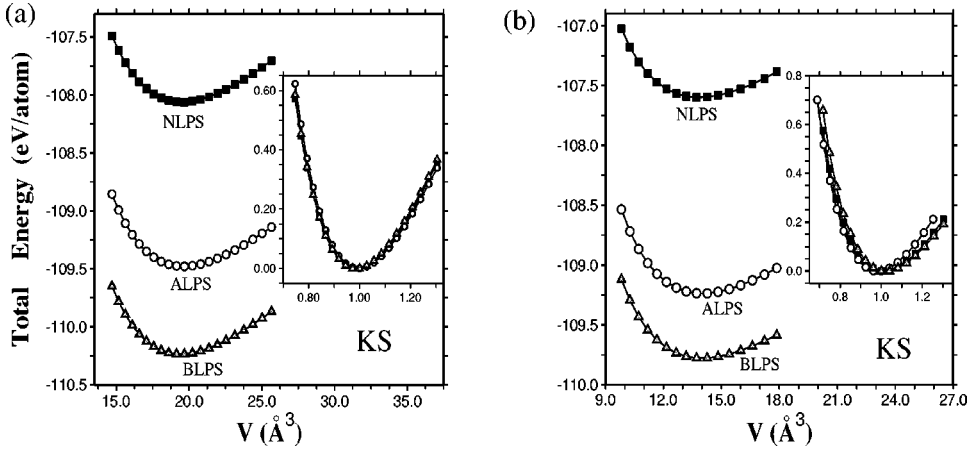


FIG. 5. LDA total energies (eV/atom) vs atomic volume (\AA^3) for CD [(a)] and fcc [(b)] Si. Both (a) and (b) are KS calculations comparing NLPS (solid squares) vs ALPS (open circles) vs BLPS (opaque triangles). Insets: the total energy is shifted by the equilibrium total energy per atom and the atomic volume is scaled, dividing by the equilibrium atomic volume.

the ALPS is derived from a spherically symmetric atomic configuration. In semiconducting Si, the bonding is directional, while in metallic Si, the bonding is more isotropic and hence more closely resembles the atomic case. Thus, the ALPS describes the metallic phases much better than the semiconducting phases, leading to energies too high for CD and HD Si and therefore too small a gap between the metallic and semiconducting phases. Despite the errors in relative energies, the bulk moduli obtained using the ALPS are generally in very good agreement with those from the NLPS (aside from the fcc Si phase, which is slightly too large).

Use of the BLPS in KS-LDA improves the relative energies markedly. The phase ordering with the BLPS is correct almost for all structures (a slight error exists between sbcc and fcc energies), though the β -tin relative energy is ~ 0.05 eV too high. The qualitative energy differences between semiconducting Si and metallic Si phases ($\Delta E \approx 0.4$ eV) are now well reproduced. Since the BLPS contains information of seven phases of bulk Si, it now treats them on more of an equal footing. The equilibrium volumes and bulk moduli predicted by the BLPS are also in reason-

able agreement with those from the NLPS; however, compared to those from the ALPS, the bulk moduli in particular are often worse. It is the relative energies of various structures that leads us to conclude that the BLPS improves upon the ALPS.

It seems a bit contradictory that the ALPS could produce as accurate PES's as the BLPS, but make severe errors in energetics. We can understand this by recognizing that the overall shape of the PES depends on the first derivative of the reciprocal space LPS $dv_{\text{LPS}}(g)/dg$ and on the value of $v_{\text{LPS}}(g=0)$. By contrast, the relative energy ordering of various phases relies on the value of $v_{\text{LPS}}(g)$ at the distinctive Bragg vectors of different structures and at $g=0$. In the case of Si, the BLPS has lower values at small g (Fig. 2), which will stabilize systems with large volume; on the other hand, lowering the $v_{\text{LPS}}(g=0)$ value will stabilize systems with small volume. By carefully balancing these competing factors, the BLPS can be constructed to minimize the error engendered by the ALPS in energetics, while maintaining the accurate shape of the PES produced by the ALPS.

When constructing the BLPS, no information from the

TABLE IV. Comparison of KS-LDA predictions of Si bulk properties for three different pseudopotentials: equilibrium volume (V_0), bulk modulus (B_0), equilibrium total energy for CD Si (E_{min}), and equilibrium total energy relative to CD Si ($\Delta E_{\text{min}} = E_{\text{min}} - E_{\text{min}}^{\text{CD}}$) for other bulk phases.

	CD	HD	cbcc	β -tin	bct5	sc	hcp	sbcc	fcc
NLPS									
$V_0(\text{\AA}^3)$	19.532	19.579	17.735	14.796	16.871	15.499	13.765	14.057	13.850
$B_0(\text{GPa})$	92.5	89.2	90.8	114.7	98.2	105.0	89.0	96.6	86.7
$(\Delta)E_{\text{min}}(\text{eV/atom})$	-108.059	0.014	0.137	0.228	0.246	0.293	0.435	0.446	0.461
ALPS									
$V_0(\text{\AA}^3)$	19.643	19.692	17.812	14.754	16.846	15.440	13.852	13.993	14.025
$B_0(\text{GPa})$	93.0	89.4	89.2	113.2	98.7	106.6	91.8	99.7	95.6
$(\Delta)E_{\text{min}}(\text{eV/atom})$	-109.477	0.017	0.122	0.108	0.166	0.170	0.227	0.237	0.241
BLPS									
$V_0(\text{\AA}^3)$	19.432	19.492	17.850	14.880	16.838	15.537	13.858	14.058	14.022
$B_0(\text{GPa})$	95.5	91.5	90.0	106.5	97.5	103.0	83.0	88.6	87.8
$(\Delta)E_{\text{min}}(\text{eV/atom})$	-110.234	0.020	0.165	0.275	0.249	0.303	0.447	0.462	0.457

TABLE V. Transition pressures (GPa) calculated from KS-LDA using the TM NLPS, the ALPS and the BLPS. Values in parentheses are the corresponding OF-LDA results using the WGC KEDF.

	NLPS	ALPS	BLPS	Expt
CD→ β -tin	8.2	3.6 (6.4)	10.2 (12.0)	12.5 ^a
CD→bct5	16.3	10.1 (17.0)	16.6 (23.0)	

^aFrom Ref. 43.

cbcc (Ref. 36) and bct5 (Ref. 34) phases were used. Therefore, calculation of their properties provides a good test of the transferability of the BLPS. KS-LDA results for those phases are also shown in Table IV. The relative equilibrium total energy, equilibrium volume, and bulk modulus of the cbcc phase obtained from the NLPS are reasonably well reproduced by both the ALPS and the BLPS. For the bct5 structure, again the NLPS equilibrium volume and the bulk modulus are reproduced well by both the ALPS and the BLPS. The marked improvement again appears in the relative energy, when the BLPS yields almost exactly the NLPS result, while the ALPS relative energy is too low (as in all the metallic cases calculated with the ALPS).

3. Pressure-induced phase transitions

Up to now, we have only considered structural properties at zero temperature and pressure. At nonzero temperature and pressure, the stability of a system depends on the Gibbs free energy

$$G \equiv E_{\text{total}} + PV - TS. \quad (26)$$

At zero temperature, pressure can cause the Gibbs free energy of different phases to change and lead to pressure-induced phase transitions. Table V displays transition pressures at zero K calculated with KS-LDA and OF-LDA using the NLPS, the ALPS, and the BLPS, and employing the common tangent rule

$$\left. \frac{dE}{dV} \right|_{\text{phase1}} = \left. \frac{dE}{dV} \right|_{\text{phase2}} = -P_{\text{trans}}. \quad (27)$$

Within KS-LDA, the phase transition from CD to β -tin Si occurs at 8.2, 3.6, and 10.2 GPa, using the NLPS, ALPS, and BLPS, respectively, while the experimental value at room temperature is 12.5 GPa (Ref. 43) (see also Ref. 35). Here again we see the superiority of the BLPS over the ALPS, with the BLPS yielding the pressure closest to both experiment and the NLPS value. For the transition from CD to bct5, the corresponding values are 16.3, 10.1, and 16.6 GPa from the NLPS, ALPS, and BLPS, respectively. No experimental data are available for this transition, but the excellent agreement between the BLPS and the NLPS is encouraging.

4. Vacancy and self-interstitial formation energies in Si

We also tested the transferability of these local pseudopotentials by studying defects in CD Si. Here we consider both formation of a vacancy and a self-interstitial, whose formation energies are calculated as

TABLE VI. Defect formation energy (eV/defect) calculated from KS-LDA for CD Si.

	NLPS	ALPS	BLPS	other estimates
vacancy	3.67	3.21	3.17	3.6 ^a
self-interstitial	3.99	3.14	3.46	3.76 ^b

^aFrom Ref. 44—experimental estimate.

^bFrom Ref. 45—KS-LDA, larger supercell, relaxed structure.

$$E_{vf} \equiv E \left(N-1, 1, \frac{N-1}{N} \Omega \right) - \frac{N-1}{N} E(N, 0, \Omega), \quad (28)$$

$$E_{if} \equiv E \left(N+1, 1, \frac{N+1}{N} \Omega \right) - \frac{N+1}{N} E(N, 0, \Omega), \quad (29)$$

where $E(n, m, \Omega)$ is the total energy of the system of volume Ω , with n Si atoms and m defects. The results are shown in Table VI. For comparison, we also list the vacancy formation energy estimated by Watkins *et al.* from their experimental work,⁴⁴ and a KS-LDA self-interstitial formation energy by Needs.⁴⁵ Since we do not allow the defective crystals to relax, the results obtained here are only rough approximations to the true defect formation energy. For the vacancy formation energy, our approximate result from KS-NLPS is very close to the experimental result, while results from both the ALPS and the BLPS are too small by ~ 0.5 eV. For the self-interstitial formation energy, the NLPS prediction is only slightly larger than that obtained from a more refined KS-LDA calculation in which a larger relaxed supercell was employed.⁴⁵ Again, the ALPS and the BLPS yield values that are ≥ 0.5 eV too small, but the BLPS is a clear improvement here over the ALPS.

C. Application of the pseudopotential in bulk environments with OF-DFT

As stated earlier, the ultimate goal is to create high quality local pseudopotentials for use in OF-DFT calculations. Having established the accuracy of the BLPS in KS-DFT, we now apply the ALPS and the BLPS in OF-LDA.

1. The density

In OF-DFT, the variationally optimized density is the most important feature to measure the quality of the KEDF and the LPS. In Table VII, we compare the OF-LPS density to the KS-NLPS density, again by calculating the four energy differences established before. As expected, the deviations in these quantities are larger for OF-DFT than for KS-DFT (Table III). In general, we see that the BLPS produces a better density than the ALPS in all three structures. It is very encouraging that the OF-BLPS density for CD Si is remarkably accurate. The bct5 phase exhibits larger deviations in the density. Given the accuracy of the KS-LPS density, it is likely that this error is caused by the WGC KEDF. An explicit comparison of KS and OF densities for CD Si is given in Fig. 4(b) for a density slice along the diagonal of the (110)

TABLE VII. Deviations of the LPS OF densities from the NLPS KS-LDA density for CD, bct5, and fcc Si, as characterized by the four energy differences (meV/atom) described in the text. The OF-DFT calculations used the WGC KEDF.

	ΔJ	$J[\Delta\rho]$	ΔE_{xc}	$\Delta\langle v_{xc} \rho\rangle$
ALPS				
CD	-216.77	4.83	69.46	91.05
bct5	-558.64	46.84	243.60	320.11
fcc	-9.97	0.84	2.93	3.85
BLPS				
CD	86.59	4.49	-26.58	-35.08
bct5	-413.50	35.93	196.18	257.80
fcc	21.36	0.48	-10.81	-14.21

plane. Both the ALPS and the BLPS put a bit too much density in the bonding region [$1.5 \lesssim r \lesssim 3.2$ a.u.], but everywhere else the OF-LPS densities are quite close to the KS-NLPS density.

2. Static structural properties

We now use the ALPS and the BLPS to calculate the PES in OF-DFT to find out if forces can be calculated sufficiently accurately (thinking ahead to dynamical simulations). The PES's for CD and fcc Si from OF-LDA (using the ALPS and the BLPS) are plotted in Fig. 6. The insets again show the scaled results, as in Fig. 5. In these OF-DFT calculations, both the WGC and WT KEDF's were employed. We also plot the PES from KS-LDA (using the ALPS and the BLPS) for comparison. The PES's of CD Si from both KEDF's are not satisfactory [see Figs. 6(a) and 6(c)], although the improvement of the WGC KEDF over the WT KEDF is evident. First, the PES from the WGC KEDF has a distinct minimum, unlike the WT KEDF. Second, the WGC KEDF brings the total energy at different volumes much closer to the KS total energy for both the ALPS and the BLPS. At the equilibrium volume predicted in KS theory, the total energy obtained from OF-DFT is very close to that from KS-DFT for both the ALPS and the BLPS. However, for smaller volumes, the total energies are overestimated and for large volumes they are considerably underestimated. The PES's of fcc

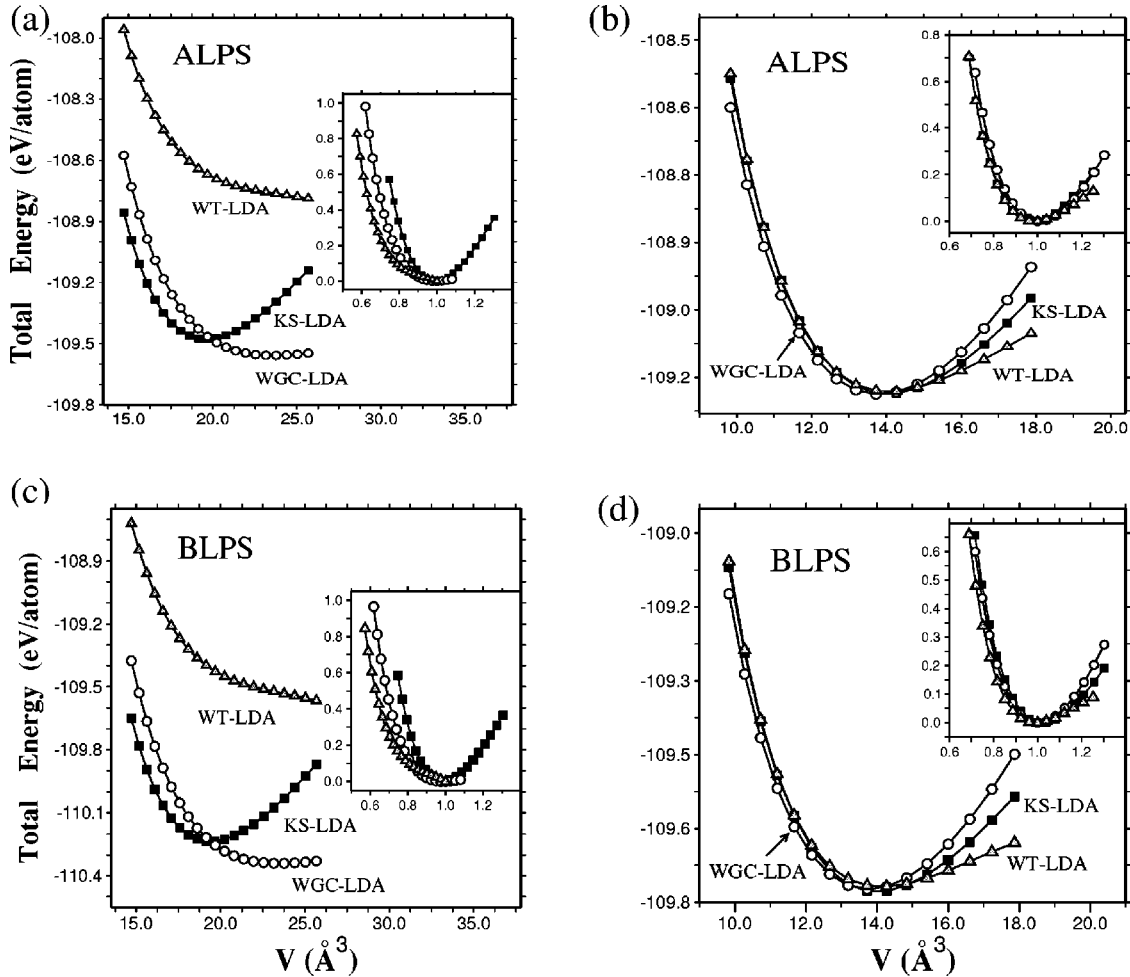


FIG. 6. LDA total energies (eV/atom) vs atomic volume (\AA^3) for CD [(a), (c)] and fcc [(b), (d)] Si. Insets: the total energy is shifted by the equilibrium total energy per atom and the atomic volume is scaled, dividing by the equilibrium atomic volume. (a) and (b) use the ALPS to compare KS (solid squares) vs OF/WGC KEDF (open circles) vs OF/WT KEDF (opaque triangles). (c) and (d) use the BLPS to compare KS (solid squares) vs OF/WGC KEDF (open circles) vs OF/WT KEDF (opaque triangles).

TABLE VIII. Comparison of OF-LDA predictions of Si bulk properties using the WGC KEDF.

	CD	HD	cbcc	β -tin	bct5	sc	hcp	sbcc	fcc
ALPS									
$V_0(\text{\AA}^3)$	23.987	19.036	17.772	14.545	16.943	15.653	13.715	13.902	13.766
$B_0(\text{GPa})$	27.2	92.6	93.9	124.3	89.7	108.2	116.1	113.9	106.4
$(\Delta)E_{\min}(\text{eV/atom})$	-109.562	0.302	0.458	0.314	0.448	0.349	0.321	0.361	0.323
BLPS									
$V_0(\text{\AA}^3)$	23.966	18.788	17.802	14.638	16.963	15.749	13.689	13.938	13.738
$B_0(\text{GPa})$	25.8	92.6	93.2	120.7	88.6	107.7	111.6	107.2	101.6
$(\Delta)E_{\min}(\text{eV/atom})$	-110.345	0.324	0.537	0.515	0.602	0.506	0.569	0.617	0.571

Si in the OF scheme are much better [see Figs. 6(b) and 6(d)], although small deviations from the KS results still exist. From the insets, we see that the ALPS and the BLPS work roughly equally well.

To obtain structural properties, the OF-DFT results are again least-squares-fitted to Murnaghan's equation of state for all nine phases of Si (Table VIII). Both the ALPS and the BLPS predict CD Si to be the ground state within OF-LDA. However, the energy ordering and magnitude of the energy differences (ΔE_{\min}) for the phases are wrong (compare Tables IV and VIII). For the ALPS, ΔE_{\min} are too high for all structures when compared against KS-LDA using the ALPS. Compared to KS-LDA using the NLPS, the ALPS-OF ΔE_{\min} are too high for the first five structures and too low for the last three. For the BLPS, again the ΔE_{\min} are too high for all phases. We also see substantial errors for CD Si in the equilibrium volume ($\sim 20\%$), the bulk modulus ($\sim 70\%$), and the equilibrium energy (~ 0.1 eV/atom). On the other hand, the equilibrium volume and the bulk modulus obtained from OF-DFT for other phases are much more accurate. The errors are within 4% for the former and 20% for the latter. Given the encouraging results obtained with KS-LDA and the BLPS, the errors in Table VIII must be due primarily to shortcomings in the KEDF. The WGC KEDF is a good compromise between accuracy and cost; however, it is still not universal enough, given that it is based on a perturbation away from the uniform electron gas. The demanding case of covalent Si is far from a mere perturbation; large errors are to be expected. How to constrain future KEDF's to treat such localized electron densities remains an outstanding issue in OF-DFT.

3. Other applications

We also calculated the transition pressure using the OF-DFT data; the results are shown in Table V. Within OF-LDA using the WGC KEDF, the transition pressures are consistently higher than from KS-LDA. Since the OF-DFT predictions of the bulk modulus and equilibrium volume of CD Si have large errors, we do not expect the transition pressures to be reliable. We believe the agreement between the OF-ALPS and the KS-NLPS transition pressures is fortuitous.

We attempted to calculate defect formation energies within OF-DFT. We find that the dramatic variation of the

density in the defect area in CD Si is beyond the range that the present KEDF's can handle, leading to unacceptably large errors in relative energies. However, we still found that the electron densities in these defective systems are better reproduced by the BLPS than by the ALPS.

VI. CONCLUSIONS

We proposed a scheme for generating *ab initio* local pseudopotentials suitable for use in condensed matter simulations, with the particular goal of eventually using them in linear-scaling OF-DFT calculations. The strategy exploits the external-potential–density connection established by Hohenberg and Kohn and utilizes densities from bulk crystals. In particular, we have shown that fairly accurate, transferable local pseudopotentials for an element that is not at all spherical nor nearly free-electron-like (e.g., Si) can be developed by inversion of the KS equations solved for bulk phases. Accurate phase orderings, equilibrium volumes, bulk moduli, densities, and good potential energy surfaces for bulk Si within KS-LDA are obtained with this bulk-derived local pseudopotential (BLPS). This BLPS produces transition pressures and defect formation energies that are qualitatively, though not quantitatively, correct. A major achievement is that the combination of the LPS's and the WGC KEDF in OF-DFT predicts the correct diamond structure ground state for bulk Si. However, other properties produced within OF-DFT with the BLPS still have significant errors, which can be rather confidently ascribed to error primarily in the KEDF's themselves. These results provide the impetus to now move forward in improving KEDF's for nonmetals, which is the next stage of our work.⁴¹

ACKNOWLEDGMENTS

We thank Drs. Derek C. Walter, Stuart C. Watson, Emily A. Jarvis, Mr. Vincent Cocula, Ms. Robin L. Hayes, and Mr. De-en Jiang for helpful discussions. Financial support for this project was provided by a DOD-MURI grant. Y.A.W. gratefully acknowledges financial support from the Natural Sciences and Engineering Research Council (NSERC) of Canada.

- ¹P. Hohenberg and W. Kohn, Phys. Rev. **136**, B864 (1964).
- ²W. Kohn and L.J. Sham, Phys. Rev. **140**, A1133 (1965).
- ³W. Yang, Phys. Rev. Lett. **66**, 1438 (1991); G. Galli and M. Parrinello, *ibid.* **69**, 3547 (1992); W. Kohn, Chem. Phys. Lett. **208**, 167 (1993); F. Mauri, G. Galli, and R. Car, Phys. Rev. B **47**, 9973 (1993); X.P. Li, R.W. Nunes, and D. Vanderbilt, *ibid.* **47**, 10 891 (1993); E.B. Stechel, A.R. Williams, and P.J. Feibelman, *ibid.* **49**, 10 088 (1994); P. Ordejón, D.A. Drabold, R.M. Martin, and M.P. Grumbach, *ibid.* **51**, 1456 (1995); J. Kim, F. Mauri, and G. Galli, *ibid.* **52**, 1640 (1995); S. Goedecker, J. Comput. Phys. **118**, 261 (1995); R. Baer and M. Head-Gordon, J. Chem. Phys. **109**, 10 159 (1998); M. Challacombe, *ibid.* **110**, 2332 (1999); C.K. Gan, P.D. Haynes, and M.C. Payne, Comput. Phys. Commun. **134**, 33 (2001); D.R. Bowler, T. Miyazaki, and M.J. Gillan, J. Phys.: Condens. Matter **14**, 2781 (2002).
- ⁴S.C. Watson and E.A. Carter, Comput. Phys. Commun. **128**, 67 (2000).
- ⁵For a recent review, see S. Goedecker, Rev. Mod. Phys. **71**, 267 (1999).
- ⁶W. Kohn, Phys. Rev. Lett. **76**, 3168 (1996).
- ⁷L.H. Thomas, Proc. Cambridge Philos. Soc. **23**, 542 (1927); E. Fermi, Rend. Accad. Nazl. Lincei **6**, 602 (1927); E. Fermi, Z. Phys. **48**, 73 (1928); P.A.M. Dirac, Proc. Cambridge Philos. Soc. **26**, 376 (1930); N.H. March, Adv. Phys. **6**, 1 (1957).
- ⁸D.A. Kirzhnits, Sov. Phys. JETP **5**, 64 (1957); C.H. Hodges, Can. J. Phys. **51**, 1428 (1973); K. Yonei and Y. Tomishima, J. Phys. Soc. Jpn. **20**, 1051 (1965); Y. Tomishima and K. Yonei, *ibid.* **21**, 142 (1966); E.K.U. Gross and R.M. Dreizler, Phys. Rev. A **20**, 1798 (1979); W. Stich, E.K.U. Gross, P. Malzacher, and R.M. Dreizler, Z. Phys. A **309**, 5 (1982); D.R. Murphy, Phys. Rev. A **24**, 1682 (1981); W. Yang, *ibid.* **34**, 4575 (1986).
- ⁹C.F. von Weizsäcker, Z. Phys. **96**, 431 (1935); N.H. March and W.H. Young, Proc. Soc. London Phys. Sect. A **72**, 182 (1958); P.K. Acharya, L.J. Bartolotti, S.B. Sears, and R.G. Parr, Proc. Natl. Acad. Sci. U.S.A. **77**, 6978 (1980); B.M. Deb and S.K. Ghosh, Int. J. Quantum Chem. **23**, 1 (1983); C. Herring, Phys. Rev. A **34**, 2614 (1986).
- ¹⁰J.A. Alonso and L.A. Girifalco, Phys. Rev. B **17**, 3735 (1978); M.D. Glossman, A. Rubio, L.C. Balbás, and J.A. Alonso, Int. J. Quantum Chem. Symp. **26**, 347 (1992); M.D. Glossman, A. Rubio, L.C. Balbás, J.A. Alonso, and Ll. Serra, Int. J. Quantum Chem. **45**, 333 (1993); M.D. Glossman, A. Rubio, L.C. Balbás, and J.A. Alonso, Phys. Rev. A **47**, 1804 (1993); M.D. Glossman, L.C. Balbás, A. Rubio, and J.A. Alonso, Int. J. Quantum Chem. Symp. **49**, 171 (1994).
- ¹¹E. Chacón, J.E. Alvarellos, and P. Tarazona, Phys. Rev. B **32**, 7868 (1985); P. García-González, J.E. Alvarellos, and E. Chacón, *ibid.* **53**, 9509 (1996); P. García-González, J.E. Alvarellos, and E. Chacón, Phys. Rev. A **54**, 1897 (1996); P. García-González, J.E. Alvarellos, and E. Chacón, *ibid.* **57**, 4857 (1998); P. García-González, J.E. Alvarellos, and E. Chacón, *ibid.* **57**, 4192 (1998).
- ¹²For a recent review, see Y.A. Wang and E.A. Carter, in *Theoretical Methods in Condensed Phase Chemistry* (Kluwer, Dordrecht, 2000), Chap. 5, pp. 117–184.
- ¹³N. Govind, J. Wang, and H. Guo, Phys. Rev. B **50**, 11 175 (1994); N. Govind, J.L. Mozos, and H. Guo, *ibid.* **51**, 7101 (1995); D. Nehete, V. Shah, and D.G. Kanhere, *ibid.* **53**, 2126 (1996); V. Shah, D. Nehete, and D.G. Kanhere, J. Phys.: Condens. Matter **6**, 10 773 (1994); V. Shah and D.G. Kanhere, *ibid.* **8**, L253 (1996); V. Shah, D.G. Kanhere, C. Majumder, and D.G. Das, *ibid.* **9**, 2165 (1997); P. Blaise, S.A. Blundell, and C. Guet, Phys. Rev. B **55**, 15 856 (1997); A. Vichare and D.G. Kanhere, J. Phys.: Condens. Matter **10**, 3309 (1998); A. Aguado, J.M. López, J.A. Alonso, and M.J. Stott, J. Chem. Phys. **111**, 6026 (1999); A. Aguado, J.M. López, J.A. Alonso, and M.J. Stott, J. Phys. Chem. **105**, 2386 (2001).
- ¹⁴M. Pearson, E. Smargiassi, and P.A. Madden, J. Phys.: Condens. Matter **5**, 3321 (1993); F. Perrot, *ibid.* **6**, 431 (1994).
- ¹⁵E. Smargiassi and P.A. Madden, Phys. Rev. B **49**, 5220 (1994); E. Smargiassi and P.A. Madden, *ibid.* **51**, 117 (1995); M. Foley, E. Smargiassi, and P.A. Madden, J. Phys.: Condens. Matter **6**, 5231 (1994); M. Foley and P.A. Madden, Phys. Rev. B **53**, 10 589 (1996); B.J. Jesson, M. Foley, and P.A. Madden, *ibid.* **55**, 4941 (1997); J.A. Anta, B.J. Jesson, and P.A. Madden, *ibid.* **58**, 6124 (1998).
- ¹⁶S.C. Watson and P.A. Madden, Phys. Chem. Commun. **1**, 1 (1998).
- ¹⁷S.C. Watson, Ph.D. thesis, Oxford University, Oxford, UK, 1996.
- ¹⁸L.-W. Wang and M.P. Teter, Phys. Rev. B **45**, 13 196 (1992).
- ¹⁹Y.A. Wang, N. Govind, and E.A. Carter, Phys. Rev. B **58**, 13 465 (1998); Y.A. Wang, N. Govind, and E.A. Carter, *ibid.* **60**, 16 350 (1999); *ibid.* **64**, 089903(E) (2001).
- ²⁰W.E. Pickett, Comput. Phys. Rep. **9**, 115 (1989).
- ²¹D.R. Hamann, M. Schlüter, and C. Chiang, Phys. Rev. Lett. **43**, 1494 (1979); U. von Barth and C.D. Gelatt, Phys. Rev. B **21**, 2222 (1980); G.B. Bachelet, D.R. Hamann, and M. Schlüter, *ibid.* **26**, 4199 (1982); G.P. Kerker, J. Phys. C **13**, L189 (1980); L. Kleinman and D.M. Bylander, Phys. Rev. Lett. **48**, 1425 (1982); D. Vanderbilt, Phys. Rev. B **32**, 8412 (1985); D.R. Hamann, *ibid.* **40**, 2980 (1989); A.M. Rappe, K.M. Rabe, E. Kaxiras, and J.D. Joannopoulos, *ibid.* **41**, 1227 (1990); D.M. Bylander and L. Kleinman, *ibid.* **41**, 907 (1990); X. Gonze, P. Käckell, and M. Scheffler, *ibid.* **41**, 12 264 (1990); M. Teter, *ibid.* **48**, 5031 (1993); N.J. Ramer and A.M. Rappe, *ibid.* **59**, 12 471 (1999); I. Grinberg, N.J. Ramer, and A.M. Rappe, *ibid.* **63**, 201102 (2001).
- ²²N. Troullier and J.L. Martins, Phys. Rev. B **43**, 1993 (1991).
- ²³W.C. Topp and J.J. Hopfield, Phys. Rev. B **7**, 1295 (1973); J.A. Appelbaum and D.R. Hamann, *ibid.* **8**, 1777 (1973); M. Schlüter, J.R. Chelikowsky, S.G. Louie, and M.L. Cohen, *ibid.* **12**, 4200 (1975); Th. Starkloff and J.D. Joannopoulos, *ibid.* **16**, 5212 (1977); J. Ihm and M.L. Cohen, Solid State Commun. **29**, 711 (1979); L. Goodwin, R.J. Needs, and V. Heine, J. Phys.: Condens. Matter **2**, 351 (1990); F. Nogueira, C. Fiolhais, J. He, J.P. Perdew, and A. Rubio, *ibid.* **8**, 287 (1996); F. Nogueira, C. Fiolhais, and J.P. Perdew, Phys. Rev. B **59**, 2570 (1999).
- ²⁴S. Watson, B.J. Jesson, E.A. Carter, and P.A. Madden, Europhys. Lett. **41**, 37 (1998).
- ²⁵Y.A. Wang and E.A. Carter (unpublished).
- ²⁶R. G. Parr and W. Yang, *Density-Functional Theory of Atoms and Molecules* (Oxford University Press, New York, 1989); R.M. Dreizler and E.K.U. Gross, *Density Functional Theory: An Approach to the Quantum Many-Body Problem* (Springer-Verlag, Berlin, 1990).
- ²⁷Y. Wang and R.G. Parr, Phys. Rev. A **47**, R1591 (1993).
- ²⁸R.C. Morrison and Q. Zhao, Phys. Rev. A **51**, 1980 (1995); J.D. Talman and W.F. Shadwick, *ibid.* **14**, 36 (1976); S.H. Werden

- and E.R. Davidson, in *Local Density Approximations in Quantum Chemistry and Solid State Physics* (Plenum, New York, 1984), p. 33; A. Görling, Phys. Rev. A **46**, 3753 (1992); A. Görling and M. Ernzerhof, *ibid.* **51**, 4501 (1995); C.-O. Almbladh, U. Ekenberg, and A.C. Pedroza, Phys. Scr. **28**, 389 (1983); C.-O. Almbladh and A.C. Pedroza, Phys. Rev. A **29**, 2322 (1984); A.C. Pedroza, *ibid.* **33**, 804 (1986); A. Nagy and N.H. March, *ibid.* **39**, 5512 (1989); A. Holas and N.H. March, *ibid.* **44**, 5521 (1991); F. Aryasetiawan and M.J. Stott, Phys. Rev. B **34**, 4401 (1986); F. Aryasetiawan and M.J. Stott, *ibid.* **38**, 2974 (1988); Q. Zhao and R.G. Parr, Phys. Rev. A **46**, 2337 (1992); R.G. Parr and Q. Zhao, J. Chem. Phys. **98**, 543 (1993); Q. Zhao, R.C. Morrison, and R.G. Parr, Phys. Rev. A **50**, 2138 (1994); D.J. Tozer, V.E. Ingamells, and N.C. Handy, J. Chem. Phys. **105**, 9200 (1996); R.G. Parr and Y.A. Wang, Phys. Rev. A **55**, 3226 (1997); Y. Wang and R.G. Parr, *ibid.* **47**, R1591 (1993); R. van Leeuwen and E.J. Baerends, *ibid.* **49**, 2421 (1994); R. van Leeuwen, O.V. Gritsenko, and E.J. Baerends, in *Density Functional Theory* (Springer-Verlag, New York, 1996), Vol. 1, p. 107.
- ²⁹W.H. Press, S.A. Teukolsky, W.T. Vetterling, and B.P. Flannery, *Numerical Recipes in Fortran* (Cambridge University Press, Cambridge, 1992).
- ³⁰A.P. Sutton, *Electronic Structure of Materials* (Clarendon, Oxford, 1993); W. A. Harrison, *Solid State Theory* (Dover, New York, 1980); W. A. Harrison, *Electronic Structure and the Properties of Solids* (Dover, New York, 1989).
- ³¹N.W. Ashcroft and N.D. Mermin, *Solid State Physics* (Saunders, Orlando, 1976); C. Kittel, *Introduction to Solid State Physics* (John Wiley & Sons, New York, 1996).
- ³²D.M. Ceperley and B.J. Alder, Phys. Rev. Lett. **45**, 566 (1980).
- ³³J.P. Perdew and A. Zunger, Phys. Rev. B **23**, 5048 (1981).
- ³⁴L.L. Boyer, E. Kaxiras, J.L. Feldman, J.Q. Broughton, and M.J. Mehl, Phys. Rev. Lett. **67**, 715 (1991).
- ³⁵M.T. Yin and M.L. Cohen, Phys. Rev. B **26**, 5668 (1982).
- ³⁶J. Donohue, *The Structure of the Elements* (John Wiley & Sons, New York, 1974).
- ³⁷M.C. Payne, M.P. Teter, D.C. Allan, T.A. Arias, and J.D. Joannopoulos, Rev. Mod. Phys. **64**, 1045 (1992); M.D. Segall, P.J.D. Lindan, M.J. Probert, C.J. Pickard, P.J. Hasnip, S.J. Clark, and M.C. Payne, J. Phys.: Condens. Matter **14**, 2717 (2002); M.D. Segall, C.J. Pickard, R. Shah, and M.C. Payne, Mol. Phys. **89**, 571 (1996).
- ³⁸M. Fuchs and M. Scheffler, Comput. Phys. Commun. **119**, 67 (1999).
- ³⁹H.J. Monkhorst and J.D. Pack, Phys. Rev. B **13**, 5188 (1976).
- ⁴⁰M. Ramamoorthy and S.T. Pantelides, Phys. Rev. Lett. **76**, 4753 (1996); A. Antonelli, E. Kaxiras, and D.J. Chadi, *ibid.* **81**, 2088 (1998).
- ⁴¹B. Zhou, V. L. Ligneres and E. A. Carter (unpublished).
- ⁴²F.D. Murnaghan, Proc. Natl. Acad. Sci. U.S.A. **30**, 244 (1944).
- ⁴³B.A. Weinstein and G.J. Piermarini, Phys. Rev. B **12**, 1172 (1975).
- ⁴⁴G.D. Watkins and J.W. Corbett, Phys. Rev. A **134**, 1359 (1964); S. Dannefaer, P. Mascher, and D. Kerr, Phys. Rev. Lett. **56**, 2195 (1986).
- ⁴⁵R.J. Needs, J. Phys.: Condens. Matter **11**, 10 437 (1999).